A look inside the body of a *BCR-ABL1*—like acute lymphoblastic leukemia patient: the first case report highlighting the continued relevance of autopsy practice

TO THE EDITOR: B-ALL encompasses several distinct subtypes according to the current World Health Organization (WHO) classification of hemato-lymphoid neoplasms. *BCR-ABL1*–like B-acute lymphoblastic leukemia/lymphoma is a novel provisional entity in B-ALL cases characterized by genetic aberrations in cytokine receptor and/or tyrosine kinase signaling pathways, which gives it a pattern of B-ALL with *BCR-ABL1* on gene expression profiling; however, there is no t(9;22) on cytogenetic or molecular genetic analysis [1]. This category has been assigned as a high-risk prognostic subgroup with dismal outcomes [2].

Several studies have described the clinical, biochemical, microbiological, radiological, and histopathological profiles of *BCR-ABL1*–like ALL. However, currently, there are no autopsy data available for this entity. To the best of our knowledge, this is the first autopsy report of an adult patient with *BCR-ABL1*–like ALL.

A 29-year-old man was symptomatic with progressive fatigue for six months and fever for one month. The patient had pallor and moderate splenomegaly on clinical examination. His complete blood count (CBC) revealed a hemoglobin level of 78 g/L, platelet count of 9×10^9/L, and white blood cell (WBC) count of 7.2×10^9/L with 63% circulating blasts. Bone marrow aspirate showed 94% blasts. Flow cytometry results were consistent with a diagnosis of B-ALL. The genet-
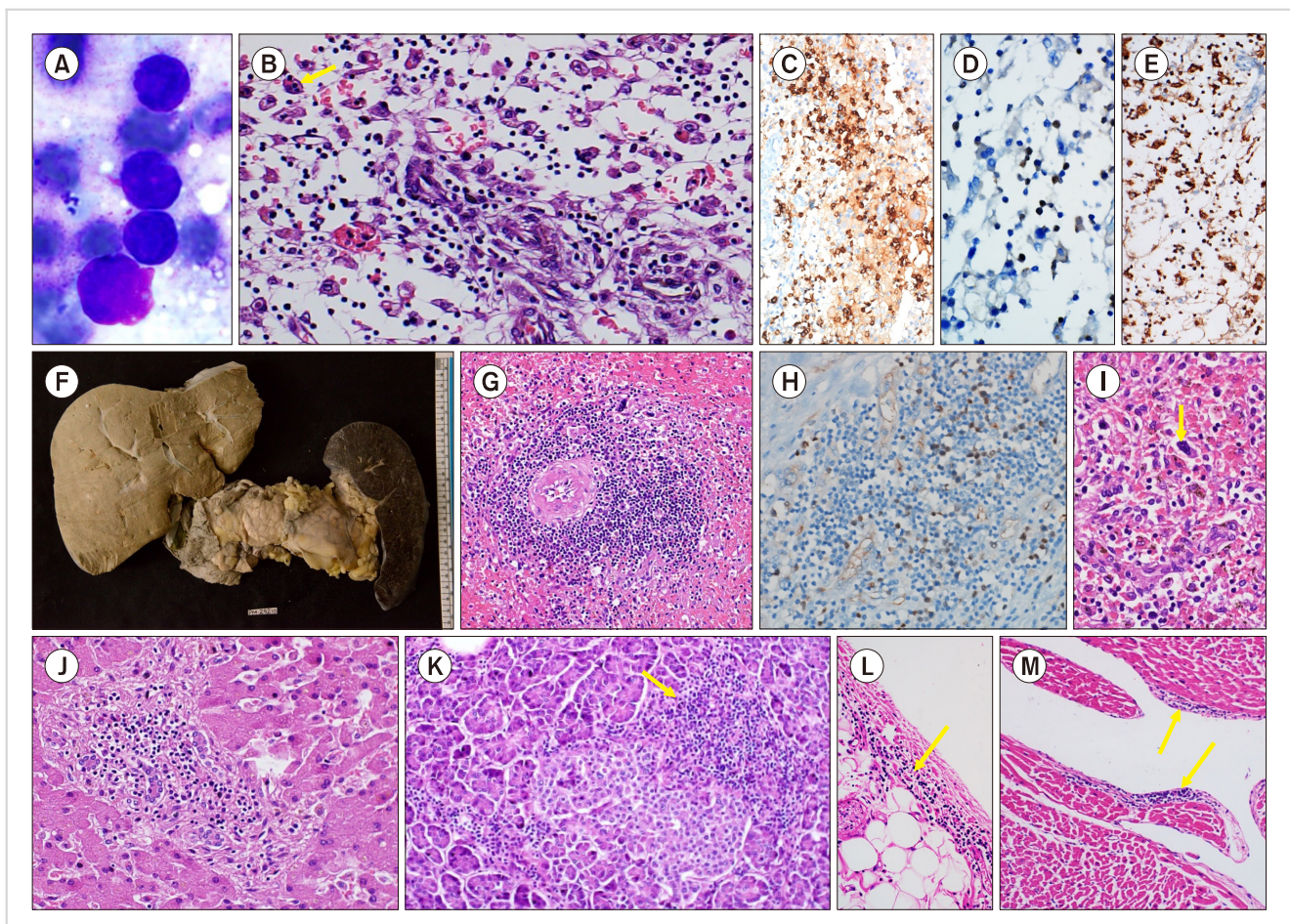
Fig. 1. Spectrum of the pathological changes seen for the basic underlying disease during autopsy. Touch imprint smears made from postmortem bone marrow biopsy showing blasts with coarse chromatin and scanty cytoplasm (**A**, ×1,000). Section of bone marrow biopsy (**B**, ×400) showing dispersed blasts, marrow edema, congested sinusoids, and hemophagocytosis (yellow arrow). Immunohistochemistry (IHC) for CD20, TdT, and CD68, respectively, highlighting blasts and increased histiocyte count (**C**–**E**, ×400). (**F**) Gross photograph of the organ complex comprising a slice of the liver, C-loop of the duodenum, pancreas, and a slice of the spleen (mildly enlarged). White of spleen is preserved (**G**, ×200) but shows scattered TdT positive cells on IHC (**H**, ×400). (**I**) The red pulp of spleen shows extramedullary hematopoiesis (arrow indicates a megakaryocyte, ×400). Portal tracts are mildly expanded due to blast infiltration (**J**, ×200). (**K**) Pancreatic acinar tissue shows leukemic infiltrates (yellow arrow, ×200). (**L**) Pericardium and endocardium (**M**) showing leukemic infiltrates (yellow arrows, ×200).

ic analysis of four common recurrent genetic aberrations [namely, t(1;19), t(9;22), t(12;21), and t(4;11)] was negative using reverse-transcriptase polymerase chain reaction. Pre-phase steroid administration was commenced according to the modified Berlin-Frankfurt-Munster (BFM) protocol. He was also administered acyclovir, trimethoprim-sulfamethoxazole, and fluconazole prophylaxis. A week later, he presented with fever, vomiting, one episode of hematemesis, difficulty in swallowing, abdominal pain, and loose stools. Abdominal examination was soft, with the spleen palpable 4 cm below the left costal margin. There was blunting of the cardiophrenic angles on chest radiography. Abdominal ultrasound revealed mild thickening of the gastric antrum, likely to be inflammatory, with kidney sizes of 11.3 and 12 cm. His CBC at this point showed a hemoglobin level of 47 g/L, WBC count of 0.4×10^9/L, and platelet count of

5×10^9/L. His creatinine level increased from 0.87 to 1.27 mg/dL. His serum electrolytes were potassium: 4.2 mEq/L, corrected calcium: 7.7 mg/dL, and phosphate: 5.1 mEq/L. He was managed for febrile neutropenia with cefoperazone-sulbactam, azithromycin, intravenous fluids, pantoprazole, and blood and platelet transfusions. Despite this, he progressed to septic shock and sustained cardiac arrest within 60 hours of presentation. The cause of death was attributed to respiratory failure, which was likely due to aspiration pneumonia, septic shock, and febrile neutropenia. There was also a clinical possibility of necrotizing enterocolitis and transfusion-related acute lung injury (TRALI). A partial (abdominothoracic) autopsy was conducted for the clinicopathological correlation.

At autopsy, effusions were present in the abdominal (2,000 mL) and bilateral pleural (1,000 mL together) cavities. The
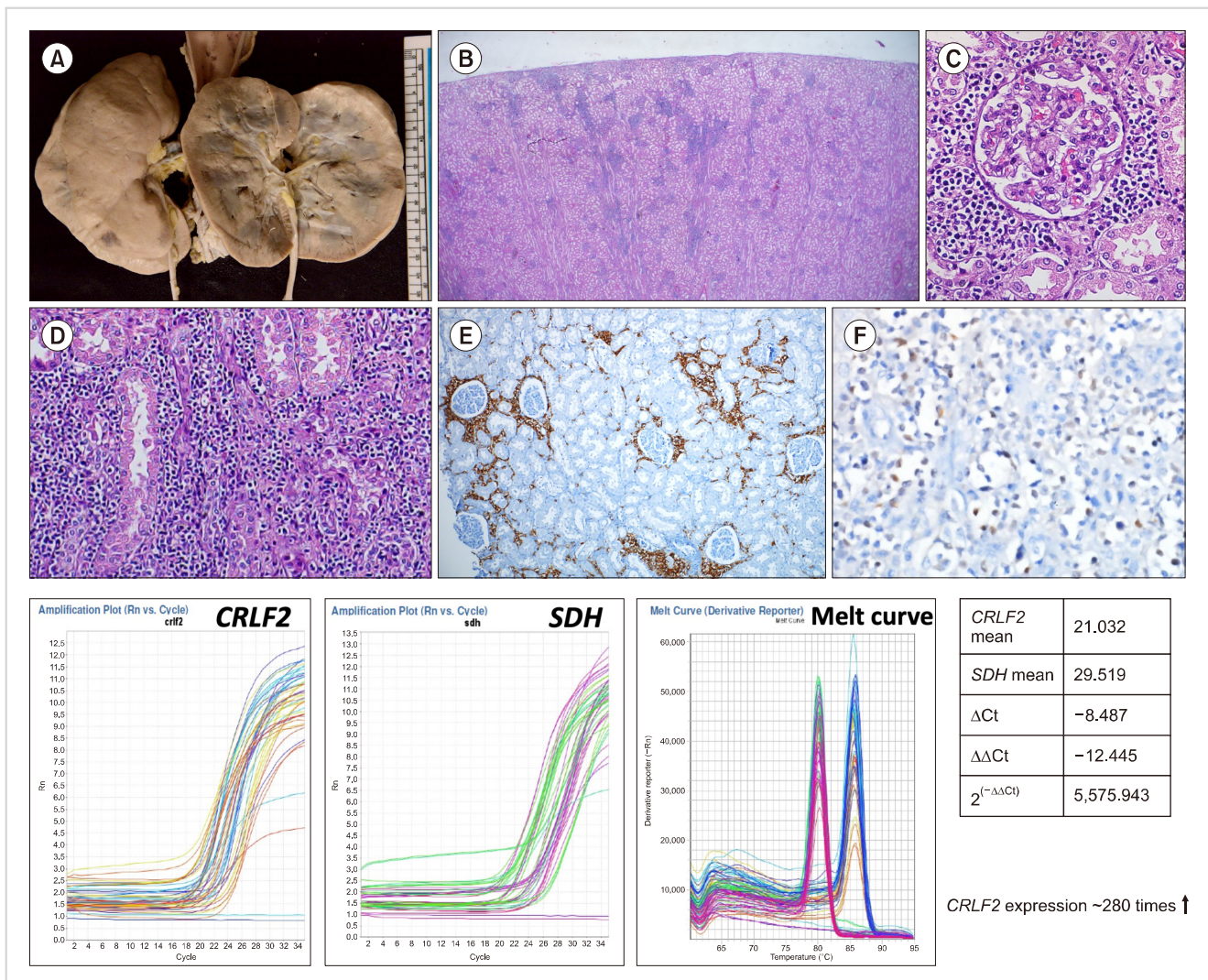
Fig. 2. Renal pathology of the case. Gross photograph of both the kidneys showing unremarkable morphology (**A**). An image (×40) of renal tissue showing the extent of leukemic infiltrates, which are highlighted by hematoxylin (blue areas, **B**). There are peri-glomerular leukemic infiltrates (**C**, ×400). Leukemic infiltrates are also seen in renal interstitium (**D**, ×400). Immunohistochemistry for CD20 and TdT, highlighting the blasts. Bottom row depicts the qRT-PCR results performed using leukemic infiltrates in renal tissue for *CRLF2* (gene of interest) and *SDH* (internal control), and the melting curve analysis demonstrates that *CRLF2* is expressed approximately 280 times more than that in the control (**E, F**).

bone marrow revealed 95% blasts along with hemophagocytosis and marrow edema (Fig. 1A–E). Enlarged para-aortic LNs with leukemic infiltrates and hemophagocytosis were also noted. The spleen was enlarged, weighing 370 g (normal, 150–200 g) with preserved white pulp showing CD20$^+$/TdT$^+$ blasts (Fig. 1F–H). Extramedullary hematopoiesis was present in the expanded red pulp in the form of erythroid precursors and megakaryocytes (Fig. 1I). The liver weighed 1700 g (normal, 1,500–1,800 g) and was grossly unremarkable (Fig. 1F). Portal tracts on microscopy were mildly expanded (Fig. 1J) with scattered CD20$^+$/TdT$^+$ blasts. Similar leukemic infiltrates were also seen in the exocrine pancreas (Fig. 1K), visceral pericardium, and endocardium (Fig. 1L, M). Grossly, both kidneys were unremarkable, but heavy leukemic infiltrates were observed around the glomeruli and interstitium (Fig. 2).

In an attempt to further characterize B-ALL at the genetic level, DNA and RNA were extracted from formalin-fixed, paraffin-embedded renal tissue with areas of maximum leukemic infiltrates. To analyze the *BCR-ABL1*–like B-ALL genetic signature, an initial assessment was performed for cytokine receptor-like factor 2 (*CRLF2*) gene overexpression using quantitative real-time polymerase chain reaction (qRT-PCR) with the extracted RNA and cDNA synthesized material (as described previously) [3]. Multiplex ligation-dependent probe amplification analysis of genomic DNA to detect copy number alterations (CNAs) was also performed for the *BCR-ABL1*–like B-ALL genetic signature. The case was positive for *CRLF2* overexpression (∼280 times) with poor-risk CNAs, such as deletions in *IKZF1*, *JAK2*, *RB1*,
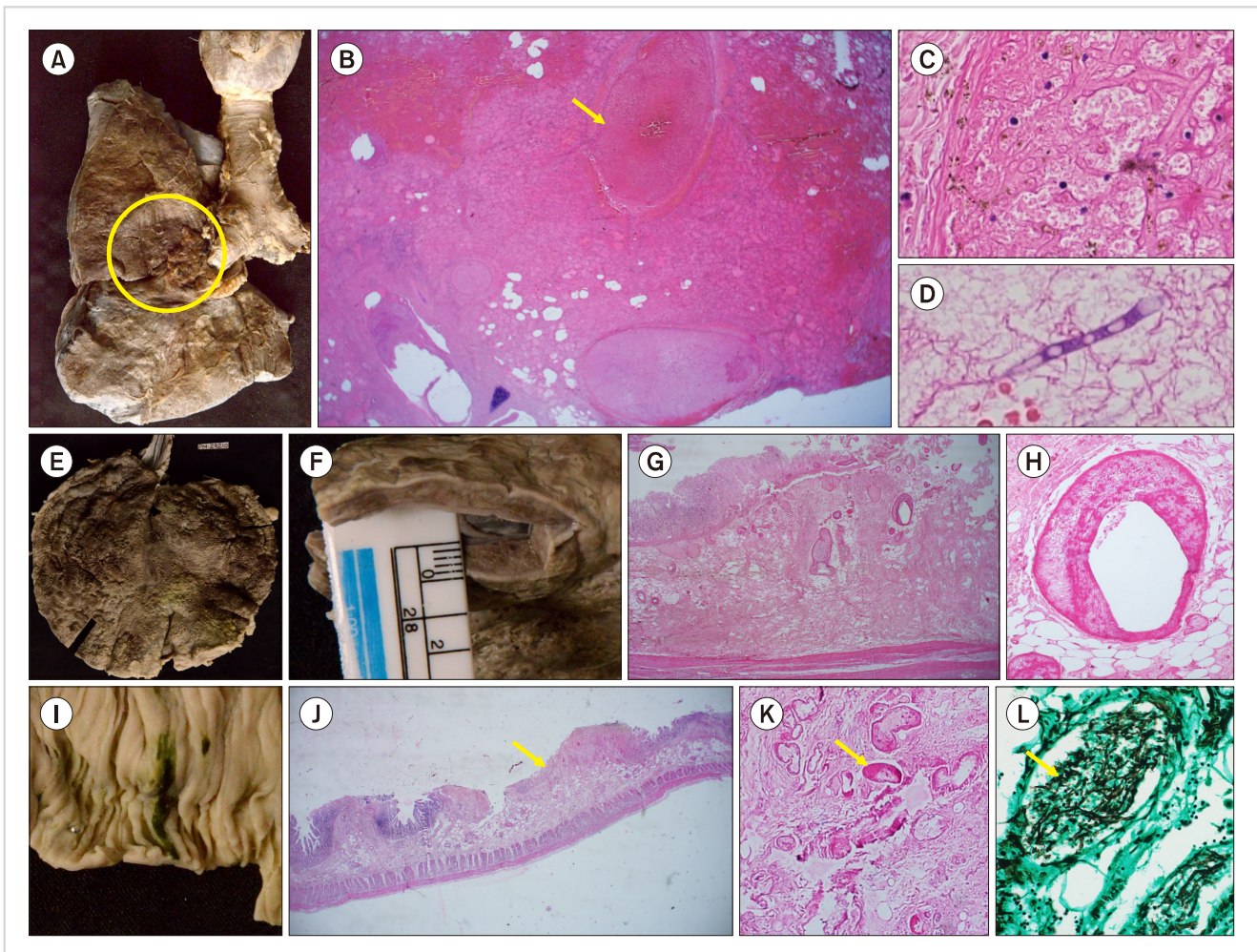
Fig. 3. Spectrum of pathologies that led to the death of patient. Gross photograph of a slice of the right lung showing a hemorrhagic area (yellow circle) near the hilum **(A)**. A large thrombus is seen in main branch of pulmonary artery (yellow arrow) with surrounding areas of hemorrhagic infarct **(B**, ×40). One of the pulmonary vessels showing fungal hyphae that are broad, aseptate, and with right-angled branching, conforming to the morphology of the *Rhizopus* species **(C**, ×400). Another focus in pulmonary parenchyma showing fungal hyphae which is straight, septate, and with no inflammatory response, conforming to the morphology of *Trichosporon* species **(D)**. Gross photographs of stomach showing diffusely ulcerated mucosa and a thickened wall (5 mm) **(E, F)**. Microscopy of stomach showing ulcerated mucosa and markedly edematous submucosa **(G**, ×100) with many thrombosed vessels **(H**, ×400). Gross image of the jejunum showing transversely oriented linear ulcers **(I)**. **(J)** Microscopy of the jejunal ulcer depicting their superficial location limited to the submucosa (yellow arrow, ×40). **(K)** The ulcer base showing fibrin thrombi in the vascular lumen (yellow arrow, ×200). **(L)** Some other vessels in submucosa showing numerous fungal profiles in lumen (Gomori Methanamine silver stain, ×400).

and *PAX5* (Fig. 2). Further characterization of *CRLF2* rearrangements and *JAK2* mutations was technically noncontributory. However, in view of *CRLF2* overexpression and the detected CNAs, the case was finally labelled as *BCR-ABL1*–like B-ALL (WHO 2016 classification).

Both the lungs demonstrated diffuse consolidation, and major vessels had thrombi around the area of hemorrhage (Fig. 3A, B). During the microscopic examination, the thrombi revealed a fungal profile (Fig. 3C), which was identified as Rhizopus species on molecular subtyping. Moreover, some other fungal hyphae conforming to the morphology of *Trichosporon* species (Fig. 3D) were also identified. Other pulmonary pathologies were an evidence of bronchopneumonia with gram-positive organisms, terminal aspiration in bronchioles, and focal leukemic infiltrates. The stomach wall was diffusely thickened (5 mm) and ulcerated (Fig. 3E, F). On microscopy, the submucosa was extensively edematous and had fibrin thrombi in the vessels, but there was no evidence of any infection or leukemic infiltrates. These findings are consistent with acute phlegmonous gastritis (Fig. 3G, H). The jejunum showed multiple transversely oriented linear ulcers (Fig. 3I). Histopathological examination revealed superficial ulcers limited to the submucosa (Fig. 3J, K). The vessels surrounding these ulcers showed fibrin thrombi, and many of them were clogged with fungal hyphae (Fig. 3L) of the *Aspergillus* species (morphologically). The remaining dissected organs were unremarkable.

Acute leukemias have heterogeneous clinical presentations, laboratory features, and varied responses to established therapies. The main diagnostic modalities are peripheral blood and bone marrow examination, together with the necessary baseline biochemical and radiological investigations. Assessment of response to therapy is usually assessed using follow-up blood counts, bone marrow remission status, and minimal residual disease estimation using flow cytometry and/or molecular markers. Even after assessing all these parameters, patients may not undergo remission or show a relapse. As it is a systemic disease, accurate assessment of residual disease (which may be extramedullary) and other confounding factors such as infections may be missed or overlooked. These cases may ultimately demonstrate dismal outcomes.

The practice of autopsy pathology has been an invaluable tool to understand the etiopathogenesis. Much of the current knowledge regarding the various aspects of different diseases is a result of vivid and varied descriptions by pioneers in the field of autopsy pathology. The original studies describing autopsy cases of hematological malignancies have been published in the English literature in the 1980s [4]. Since then, there have been significant advances in diagnostic criteria and management protocols for this disease. There is only one recent study describing the autopsy pathologies of cases of acute myeloid leukemia and non-Hodgkin lymphoma, which has shed light on the new findings [5]. Hence, there is a need to revisit autopsy pathology in cases of hematological malignancies, especially in the current era

of hematopoietic stem cell transplantation and other advanced therapeutic modalities.

The current case report describes the autopsy findings for the first time in the literature. Although the case was managed according to the hospital guidelines, the patient still succumbed to his illness, and the autopsy revealed certain pathologies that were not thought of during his life, which could have been managed. In this case, the active disease burden was also seen outside the lymphoreticular system in the form of heavy leukemic infiltrates in the kidneys, portal tracts, exocrine pancreas, and heart. Previous autopsy studies during the 1960s and 70s have also reported malignant infiltration in these extramedullary sites; however, the underlying mechanism remains unknown [5]. This can be attributed to the limited understanding of the molecular aspects of the heterogeneous nature of acute leukemias. In light of recent developments in the understanding of this disease, the mechanisms of disease progression are being explored. The migration capabilities of leukemic cells into the extramedullary sites are related to the expression and orchestration of adhesion molecules, such as CD44 and P/E-selectins, and chemokines and their receptors [6]. According to the current understanding of *BCR-ABL1*–like B-ALL, *CRLF2* overexpression activates the JAK/STAT and PI3K signaling pathways [7]. The exact mechanisms linking these pathways to the augmented expression of adhesion- and migration-related molecules remain to be elucidated.

The other significant aspect for the case was a clinicopathological miscorrelation seen with regards to pulmonary and gastrointestinal pathology. TRALI and necrotizing enterocolitis were thought to be fungal infections and acute phlegmonous gastritis. These pathologies are rapidly fatal and require prompt measures for management [8, 9]. Autopsy revealed different morphological subtypes of fungal species, which may require a different therapeutic approach [8]. Hence, this report revealed certain aspects that might be encountered in *BCR-ABL1*–like B-ALL patients, which could be responsible for its high-risk category. This need to be further elucidated by large autopsy studies.

Another aspect of this case is the potential of the autopsy material, which was utilized in the diagnosis of *BCR-ABL1*–like B-ALL. Appropriate attempts were strategically made from renal leukemic infiltrates for molecular genetic analysis to further characterize this case. Targeted therapies are now available for *BCR-ABL1*–like B-ALL subtype that lead to better outcomes [10]. Furthermore, the molecular characterization of fungal infection (*Rhizopus* species) was also investigated using autopsy material.

In summary, we describe the first report of a *BCR-ABL1*–like B-ALL case emphasizing the use of autopsy practice to further understand the pathobiology of hematological malignancies. The clinicopathological correlation was analyzed to gain insights into this entity. Certain learning points were the pattern of leukemic infiltrates, the plethora of fungal infections, and the use of autopsy material for ancillary techniques.

Pulkit Rastogi[1], Prateek Bhatia[2], Sreejesh Sreedharanunni[3], Deepesh Lad[4]

[1]Department of Histopathology, Post Graduate Institute of Medical Education & Research, [2]Department of Pediatrics, Pediatric Hematology Oncology Unit & PHO Molecular Lab, Post Graduate Institute of Medical Education & Research, [3]Department of Hematology, Post Graduate Institute of Medical Education & Research, [4]Department of Internal Medicine (Adult Clinical Hematology Unit), Post Graduate Institute of Medical Education & Research, Chandigarh, India

Correspondence to: Deepesh Lad

Department of Internal Medicine, Post Graduate Institute of Medical Education & Research, Chandigarh 160012, India E-mail: deepesh.lad12@gmail.com

Authors' Disclosures of Potential Conflicts of Interest

No potential conflicts of interest relevant to this article were reported.

REFERENCES

1. Arber DA, Orazi A, Hasserjian R, et al. The 2016 revision to the World Health Organization classification of myeloid neoplasms and acute leukemia. Blood 2016;127:2391-405.
2. Jain N, Roberts KG, Jabbour E, et al. Ph-like acute lymphoblastic leukemia: a high-risk subtype in adults. Blood 2017;129:572-81.
3. Totadri S, Singh M, Trehan A, Varma N, Bhatia P. Keeping PACE with Ph positive to Ph-like detection in B-lineage acute lymphoblastic leukemia: a practical and cost effective (PACE) approach in a resource constrained setting. Indian J Hematol Blood Transfus 2018;34:595-601.
4. Thiele J, Laubert A, Vykoupil KF, Georgii A. Autopsy and clinical findings in acute leukemia and chronic myeloproliferative diseases--an evaluation of 104 patients. Pathol Res Pract 1985;79:328-36.
5. Van de Louw A, Lewis AM, Yang Z. Autopsy findings in patients with acute myeloid leukemia and non-Hodgkin lymphoma in the modern era: a focus on lung pathology and acute respiratory failure. Ann Hematol 2019;98:119-29.
6. Vadillo E, Dorantes-Acosta E, Pelayo R, Schnoor M. T cell acute lymphoblastic leukemia (T-ALL): new insights into the cellular origins and infiltration mechanisms common and unique among hematologic malignancies. Blood Rev 2018;32:36-51.
7. Tasian SK, Loh ML. Understanding the biology of *CRLF2*-over-expressing acute lymphoblastic leukemia. Crit Rev Oncog 2011;16:13-24.
8. Bhatt VR, Viola GM, Ferrajoli A. Invasive fungal infections in acute leukemia. Ther Adv Hematol 2011;2:231-47.
9. Shi D, He J, Lv M, Liu R, Zhao T, Jiang Q. Phlegmonous gastritis in a patient with mixed-phenotype acute leukemia in the neutropenia phase during chemotherapy: a case report. Medicine (Baltimore) 2019;98:e17777.
10. Chiaretti S, Messina M, Foà R. BCR/ABL1-like acute lympho-

blastic leukemia: how to diagnose and treat? Cancer 2019;125: 94-204.

Therapy-related acute myeloid leukemia in a patient with B-cell acute lymphoblastic leukemia

TO THE EDITOR: Secondary/therapy-related neoplasms, such as acute myeloid leukemia (AML) and myelodysplastic syndrome (MDS), occur infrequently in adult patients with acute lymphoblastic leukemia (ALL) [1]. Most frequently, therapy-related/secondary myeloid neoplasms are associated with breast cancer and lymphoproliferative diseases [2]. These patients frequently have complex karyotype including many structural abnormalities indicating a poor prognosis [3]. Here, we report a case of secondary AML in an adult patient with B-ALL on maintenance chemotherapy with an unusual complex karyotype.

A 60-year-old female presented in December 2015 with fever, generalized weakness, and dizziness in the last 2 months. On ultrasonography, she had mild splenomegaly. Complete blood count showed hemoglobin of 77 g/L, total leukocyte counts of 2.84×10^9/L and platelets of 70×10^9/L with 2% blasts in peripheral blood smear. Bone marrow aspirate smears were hemodiluted, showing fairly cellular imprint smears with 80% blasts (Fig. 1A). Bone marrow biopsy (Fig. 1B) showed sheets of blasts which are positive for CD10 (Dako, 56C6), PAX5 (Biogenix, ZP007) and negative for MPO and CD33 (Bio SB, RBT-CD33). On flow cytometric immunophenotyping (Fig. 1C), these blasts were positive for CD19, CD10, CD34, HLA-DR, CD22, CD71 (dim), and CD20 (partial), while they were negative for cCD3, cMPO, CD7, CD13, CD33, CD14, CD56, CD4, CD8, CD5, and CD3; these results were consistent with the diagnosis of precursor B-cell acute lymphoblastic leukemia (ALL). Karyotype at this time showed 46,XX. Real-time polymerase chain reaction for t(1;19)(q23 ;p13.3) or TCF-3-PBX1(E2A-PBX1), t(11;19)(q23;p13.3) or MLL-ENL, t(12;21)(p13;q22) or ETV6-RUNX1(TEL-AML1), t(4;11)(q21;q23) or MLL-AF4, t(9;11)(p21-22;q23) or (MLL-AF9), and BCR-ABL1 were negative. She was started on chemotherapy according to the UK ALL protocol. The chemotherapeutic drugs included in the UK ALL treatment regimen were vincristine, daunorubicin, L-asparaginase, prednisolone, and intrathecal methotrexate. Bone marrow after induction therapy was in morphological remission and minimal residual disease by flow cytometry was negative (<0.01%). In February 2017, bone marrow after consolidation therapy was also in morphological remission and minimal residual disease by flow cytometry was negative, and she was started on maintenance chemotherapy. However, in February 2019, she presented with persistent cough. Complete blood count showed hemoglobin of 85 g/L, total leukocyte count of